A New Approach to 3-D Imaging

Vignesh Devaki Murugesan

In this work, a new approach to three-dimensional (3-D) imaging using a continuously modulated electroabsorption modulator (EAM), a vertical-cavity surface-emitting laser (VCSEL) array, and a conventional complementary metal oxide semiconductor (CMOS) camera is presented. It is based on a time-of-flight method where the distance is indirectly obtained from the light intensity measured by a time-gated photon counter or charge integrator (i.e., a CMOS pixel). It is possible to acquire distance measurements for each pixel with accuracies up to few millimeters. Potential applications include augmented reality scenarios, face recognition systems in smartphones, industrial robotics, or machine vision.

1. Introduction

The acquisition of 3-D data is important for many control, navigation, and security scenarios [1]. Fast and reliable 3-D imaging has become a main requirement in commercial, industrial, and automotive applications. Currently different types of measuring techniques are available in the market for recording the 3-D information of an object or scene. Cameras for 3-D depth imaging using time-of-flight (TOF) methods have received a lot of attention recently for a number of reasons, including their low cost, compactness, and ability to obtain 3-D data at higher frame rates [2].

2. Working Principle of the Time-of-Flight Camera

2.1 Classification

Light waves based 3-D measurement techniques are broadly divided into active and passive approaches based on the source of light used, as shown in Fig. 1. Active measurement systems use a built-in illumination source (like laser or light-emitting diode) to probe the environment. Passive measurement systems rely on detecting backscattered ambient radiation to get the 3-D information [3]. Active measurement can be mainly classified in three categories:

1. Triangulation. In the triangulation technique, laser, camera, and point on the object to be measured form a triangle from which the distance is obtained.

2. Time-of-flight. Distance is measured by knowing the time difference between emitted and backscattered light wave and the velocity of light.

3. Interferometry. Distance is inferred from interference patterns of a coherent laser source. Interferometry is limited to distances approximately less than half the coherence length of the laser [3].

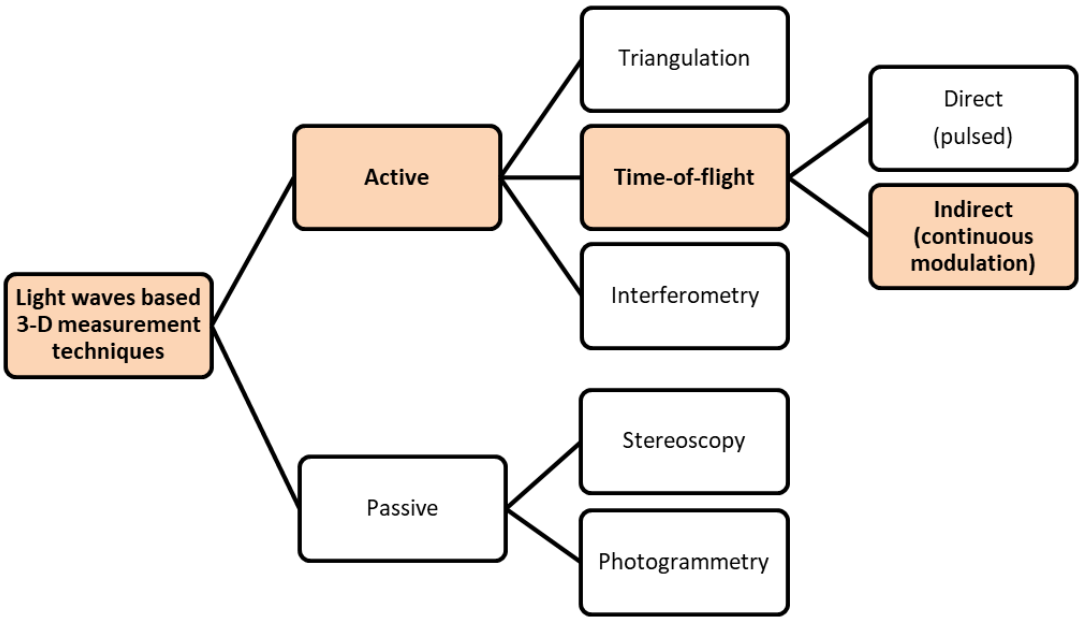

Fig. 1: Classification of non-contact 3-D surface measurement techniques based on light waves. The method discussed in this article is based on an indirect time-of-flight technique.

The TOF method is again divided into two categories:

1. Direct TOF. It is a classical TOF measurement where the time difference Δt between emitted and backscattered light waves is measured by a highly accurate stopwatch and the distance d is estimated from

$$d = \frac{c \cdot \Delta t}{2} \,, \tag{1}$$

where c is the vacuum velocity of light ($c \approx 3 \cdot 10^8\,\mathrm{m/s}$). This method is commonly used for (scanned) single-point range systems.

2. Indirect TOF. In this method the round-trip time is indirectly extracted from a time-gated measurement of a sinusoidal modulated light intensity by comparing the phase shift between outgoing and incoming signals. In this case, there is no need of a precise stopwatch, but of time-gated photon counters like, for instance, a specialized CMOS camera sensor [4]. The method introduced in this article can be classified as indirect TOF and is discussed in detail in the next section.

Important passive 3-D measurement systems in Fig. 1 include

1. Stereoscopy. Stereoscopic systems usually employ two cameras, at a fixed distance apart, looking at the same scene. By analyzing the slight differences between the images seen by each camera, it is possible to determine the distance at each point in the images.

2. Photogrammetry. It is the science of making measurements from photographs. It involves taking multiple photographs of an object from various angles and positions with a camera. Then a 3-D computer model of the object is constructed from these photographs using sophisticated algorithms.

2.2 Basic working principle

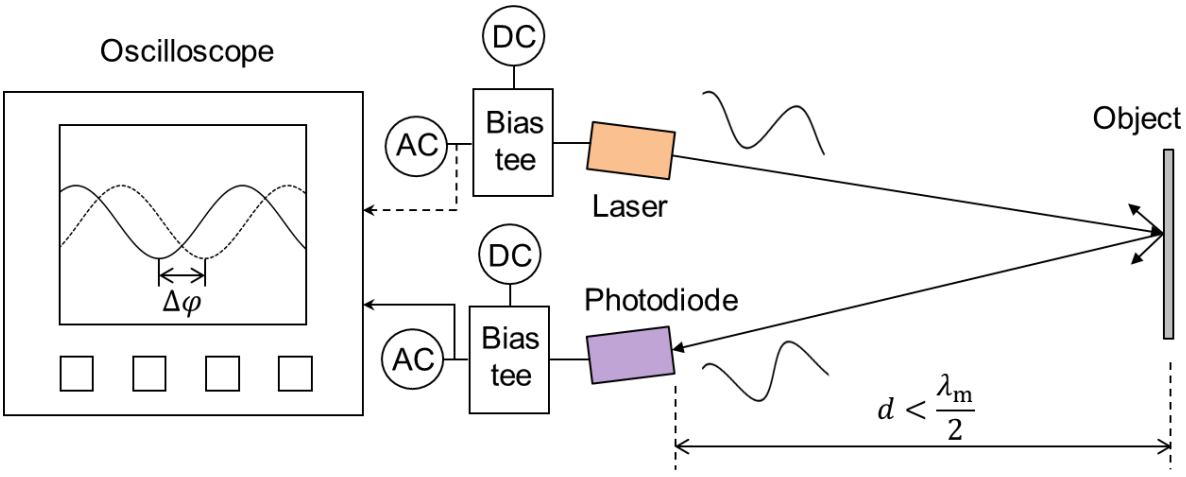

Fig. 2: Basic setup consisting of a laser modulated with a sinusoidal signal of wavelength λ_m, a photodiode, and an oscilloscope to measure the phase difference $\Delta\varphi$ between outgoing and incoming harmonic signals after light scattering at an object with distance d.

In order to explain the working principle of the method described here, one should first consider the simple setup in Fig. 2 to measure the distance of a single object point. The setup consists of a sinusoidal modulated laser and a photodiode, both with a bias tee, as well as an oscilloscope to measure the phase difference between outgoing and incoming signals. A bias tee is a passive electrical element consisting of an inductor and a capacitor that superimposes or separates direct current (DC) and alternating current (AC) signal components. The modulated laser beam is backscattered when it strikes an object at a distance d. The backscattered light from the object hits the photodiode under reverse bias and this produces an AC photocurrent with DC offset. The capacitor inside the bias tee blocks the DC and passes only the AC component to the oscilloscope. Since light has a definite speed, the light signal takes some time to travel to and from the object and the delay causes some phase shift that corresponds to the distance from the object. This phase shift $\Delta\varphi$ of the backscattered signal relative to the reference signal can be measured using an oscilloscope. The measured phase shift is proportional to the distance only if the latter is less than half the wavelength of the modulation, $d < \lambda_m/2$. Otherwise ambiguity occurs due to the harmonic nature of the signal.

This ambiguity can be better understood when one considers placing the object at a distance of exactly half the wavelength of the modulation signal, so the backscattered wave would have travelled twice the distance (i.e., to and from the object), which corresponds exactly to a distance of one wavelength of the modulation λ_m. So the backscattered wave will be in phase with the reference signal and therefore will create an ambiguity whether the object is at zero distance or at $d = \lambda_\mathrm{m}/2$. Consequently, the distance should be less than half-wavelength of the modulation. The maximum range of measurement can be increased with larger λ_m. However, a longer wavelength of the modulation results in low depth resolution because a given distance span to be measured expressed as a percentage of λ_m will be small when compared with the same span in case of a small modulation wavelength. Hence, a given device with a fixed capability to resolve phase will have higher accuracy when the distance to be measured approaches $\lambda_\mathrm{m}/2$. In order to have a flexible range of measurement and good accuracy, measurements can be done with different wavelengths of modulation with decreasing λ_m, and by processing these sets of measurements, ambiguity can be resolved.

The simple setup discussed above can be used only to measure one single point. In order to get distance values for multiple points one needs to have a 2-D array of photodiodes and each photodiode connected to a circuit or device that can measure phase, which makes the setup costly and bulky. Another solution is to mount the setup on a movable device and to scan the object or scene, but this is a time-consuming process [3].

An alternative solution is to use an electroabsorption modulator and a CMOS camera to demodulate the signal and calculate the distance, as shown in Fig. 3. Owing to its favorable characteristics [5] a VCSEL is a convenient light source for use in the 3-D imaging setup. An intensity-modulated beam from a VCSEL is expanded using a suitable lens system to illuminate a defined area. The EAM is an optoelectronic device that can vary the amount of light transmitted through it when a voltage is applied. Its working principle is discussed in detail in Sect. 3.1. The same AC signal applied to the VCSEL also modulates the EAM favorably in a synchronous way. The EAM can be placed between lens and CMOS camera sensor, as shown in Fig. 3, or can be placed in front of the lens. Light backscattered from the object is focused by the lens on the image sensor and passes through the EAM. Calculations in the next section show in detail how demodulation is done to produce precise distance measurements by using this method.

2.3 Calculation and demodulation

Figure 4 shows the light signal power at various points along the indicated path of the ray. The optical output power of a sinusoidal modulated VCSEL is

$$P_\mathrm{V}(t) = P_0 \cdot (1 + p \cdot \sin(2\pi f_\mathrm{m} t)) \ , \tag{2}$$

where P_0 is the average power when only a DC bias is applied, f_m is the frequency of the AC signal, t is the time, and the modulation coefficient p is

$$p = \frac{\Delta P}{P_0} \quad (0 \leq p \leq 1) \tag{3}$$

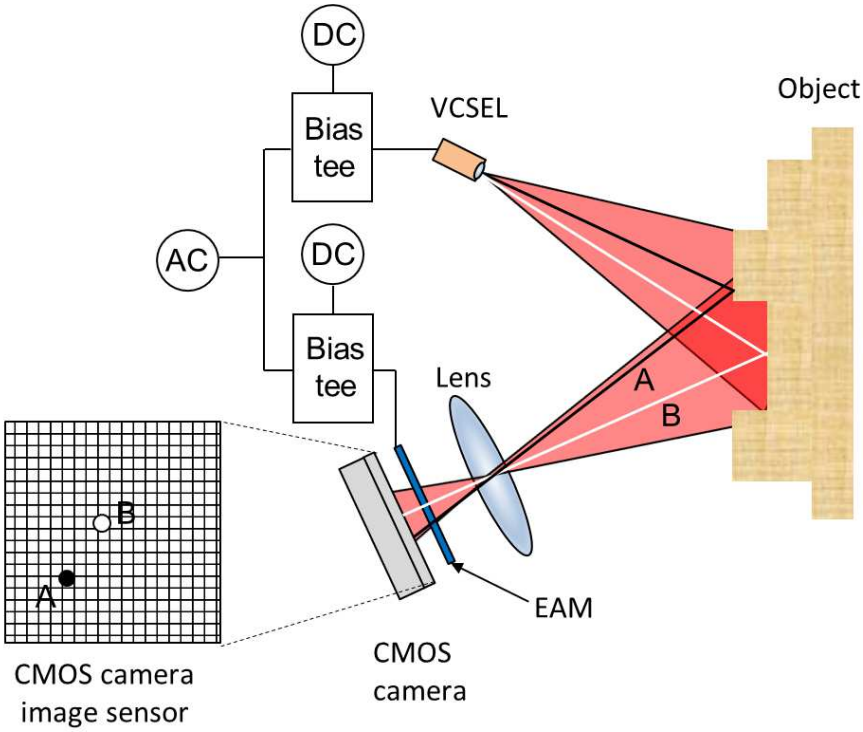

Fig. 3: 3-D measurement setup consisting of electroabsorption modulator (EAM) and CMOS camera to demodulate the signal and calculate the distance. The rays A and B hit different spots and travel different distances and therefore have different phases which are subsequently detected.

with ΔP being the modulation amplitude according to Fig. 4 (top right), where $0 \leq \Delta P \leq P_0$. In order to obtain a good signal-to-noise ratio, p should be close to 1. The light signal power backscattered by the object just before it arrives at the modulator has experienced a time delay Δt and is given by

$$P_\mathrm{r}(t) = R_0 \cdot P_\mathrm{V}(t - \Delta t) = P_0 \cdot (1 + p \cdot \sin(2\pi f_\mathrm{m} t - \Delta\varphi)) \ , \tag{4}$$

where R_0 is the ratio of the light power backscattered by the object towards the modulator to the light power emitted by the VCSEL and $\Delta\varphi$ is the modulation phase delay acquired by the wave after it has travelled a distance of $2d$, i.e., $\Delta\varphi = 2d \cdot 2\pi/\lambda_\mathrm{m}$ with $\lambda_\mathrm{m} = c/f_\mathrm{m}$. The EAM is driven with a DC-biased sinusoidal electrical signal that results in an EAM transmittance of

$$M(t) = M_0 \cdot (1 + m \cdot \sin(2\pi f_\mathrm{m} t)) \tag{5}$$

with

$$m = \frac{\Delta M}{M_0} \qquad (0 \leq m \leq 1) \ , \tag{6}$$

where M_0 is the light power ratio transmitted through the EAM when only a DC bias is applied and ΔM is the EA modulation amplitude from Fig. 4 (bottom right). Equivalent to (3), $m \approx 1$ for best signal-to-noise ratio. The light signal power transmitted by the modulator is

$$P(t) = M(t) \cdot P_\mathrm{r}(t) \tag{7}$$

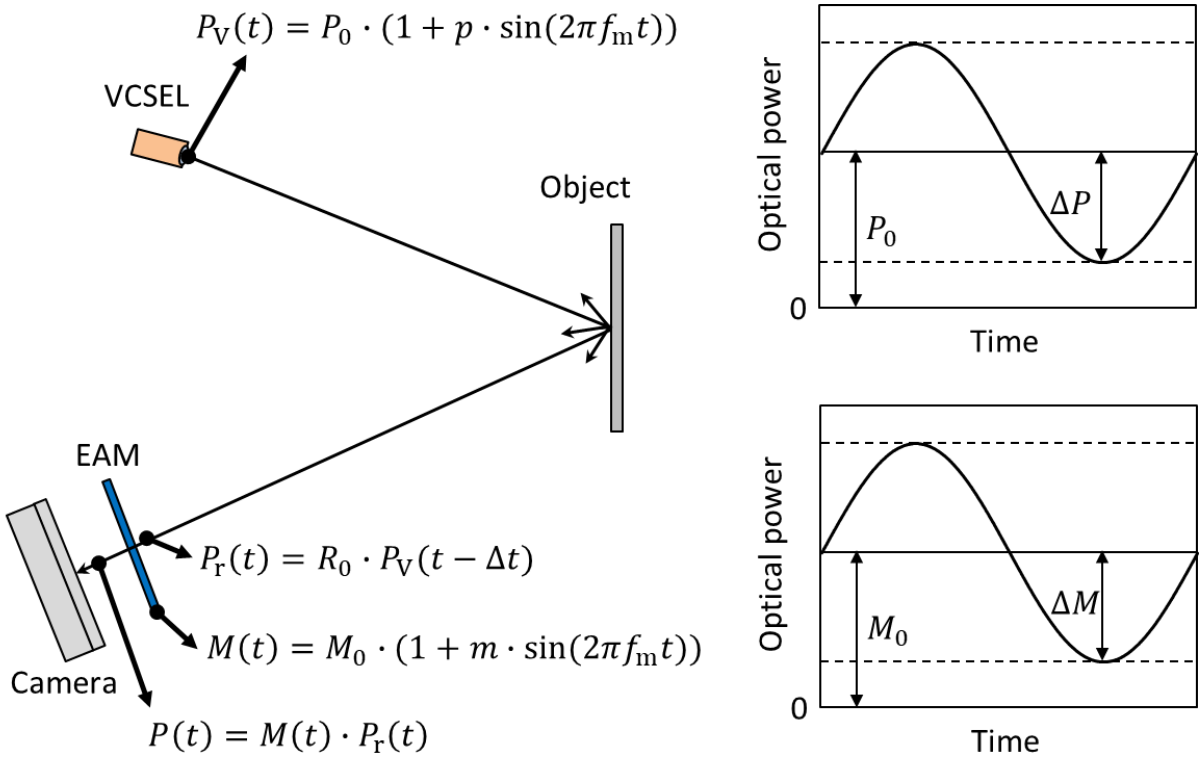

Fig. 4: Sinusoidal modulated light signal power at various points of the 3-D measurement setup in Fig. 3. Top-right and bottom-right diagrams show the time functions of VCSEL and EAM modulation, respectively.

or in explicit form

$$P(t) = P_0 R_0 M_0 \cdot (1 + m \cdot \sin(2\pi f_m t)) \cdot (1 + p \cdot \sin(2\pi f_m t - \Delta\varphi)) \ . \tag{8}$$

On applying a trigonometric theorem for the product of sine functions one obtains

$$\begin{aligned} P(t) = \frac{P_0 R_0 M_0}{2} \quad &\cdot \quad [2 + 2m \cdot \sin(2\pi f_m t) + 2p \cdot \sin(2\pi f_m t - \Delta\varphi) \\ &+ \quad mp \cdot \cos(\Delta\varphi) - mp \cdot \cos(4\pi f_m t - \Delta\varphi)] \ . \end{aligned} \tag{9}$$

When this signal is time-averaged $\langle \ldots \rangle_{\delta t}$ by the CMOS camera pixel for a specific time interval $\delta t \gg 1/f_m$, the sin and cos functions with $f_m t$ become zero. This leads to

$$P(\Delta\varphi) = \langle P(t, \Delta\varphi) \rangle_{\delta t} = \frac{P_0 R_0 M_0}{2} \cdot [2 + mp \cdot \cos(\Delta\varphi)] = A \cdot \cos(\Delta\varphi) + K \ , \tag{10}$$

where $K = P_0 R_0 M_0$ is a constant and $A = mpK/2$. Background radiation is not considered during the derivation but can be added into K assuming it remains constant over the period of integration. R_0 and $\Delta\varphi$ as well as unavoidable background radiation power are unknown in (10), so at least three measurements are required in order to find $\Delta\varphi$. Typically four samples at discrete phase offsets of 0°, 90°, 180°, and 270° of the function $P(\Delta\varphi)$ are used to sequentially acquire signals P_0, P_1, P_2, and P_3. More measurements

improve the precision but also increase the acquisition and computation time, so it is usually sufficient to evaluate the four samples [6]

$$P_0 = P(\Delta\varphi) = A \cdot \cos(\Delta\varphi) + K \ , \tag{11}$$
$$P_1 = P(\Delta\varphi + 90^\circ) = -A \cdot \sin(\Delta\varphi) + K \ , \tag{12}$$
$$P_2 = P(\Delta\varphi + 180^\circ) = -A \cdot \cos(\Delta\varphi) + K \ , \tag{13}$$
$$P_3 = P(\Delta\varphi + 270^\circ) = A \cdot \sin(\Delta\varphi) + K \tag{14}$$

and obtain

$$\tan(\Delta\varphi) = \frac{P_3 - P_1}{P_0 - P_2} \ . \tag{15}$$

Thus we arrive at

$$\Delta\varphi = \arctan \frac{P_3 - P_1}{P_0 - P_2} \ . \tag{16}$$

Phase $\Delta\varphi$ and distance d are related by

$$\Delta\varphi = \frac{2\pi}{\lambda_\mathrm{m}} 2d \ . \tag{17}$$

Since $\lambda_\mathrm{m} = c/f_\mathrm{m}$, (17) becomes

$$d = \frac{c}{4\pi f_\mathrm{m}} \Delta\varphi \ , \tag{18}$$

showing that the distance d of an object point is easily obtained by measuring the signals P_i, $i = 0, 1, 2, 3$ for every pixel of the image sensor.

3. Modulator

3.1 Working principle

The EAM works based on the principle of the quantum-confined Stark effect (QCSE). Figure 5 illustrates the band structure of a GaAs quantum well (QW) embedded in AlGaAs barriers. In the very thin ($\approx$ 10 nm) GaAs QW layer, quantum confinement of electrons and holes occurs which results in a radical modification of the optical absorption spectrum [7]. The quantum confinement changes the absorption spectrum from the smooth function of bulk material to a series of steps. Additionally, the confinement also increases the binding energy of the bound excitons, resulting in exceptionally clear exciton resonances at room temperature in GaAs–AlGaAs QWs. An exciton is a bound electron–hole pair where electron and hole are attracted by the electrostatic Coulomb force just as an electron is bound to a proton to form a neutral hydrogen atom [8]. Usually excitons in bulk GaAs are not stable at room temperature. This is because the excitons are ionized and elevated to the conduction band by phonons so fast that no resonances can develop. In contrast, GaAs QWs show excitonic resonances in absorption spectra at room temperature because the binding energy of two-dimensional excitons inside a QW in the ideal case is four times greater than in bulk material [9].

If a static electric field is applied perpendicular to the plane of the QW, the bands tilt and the potential profile is changed, as shown in the right part of Fig. 5. The deformation

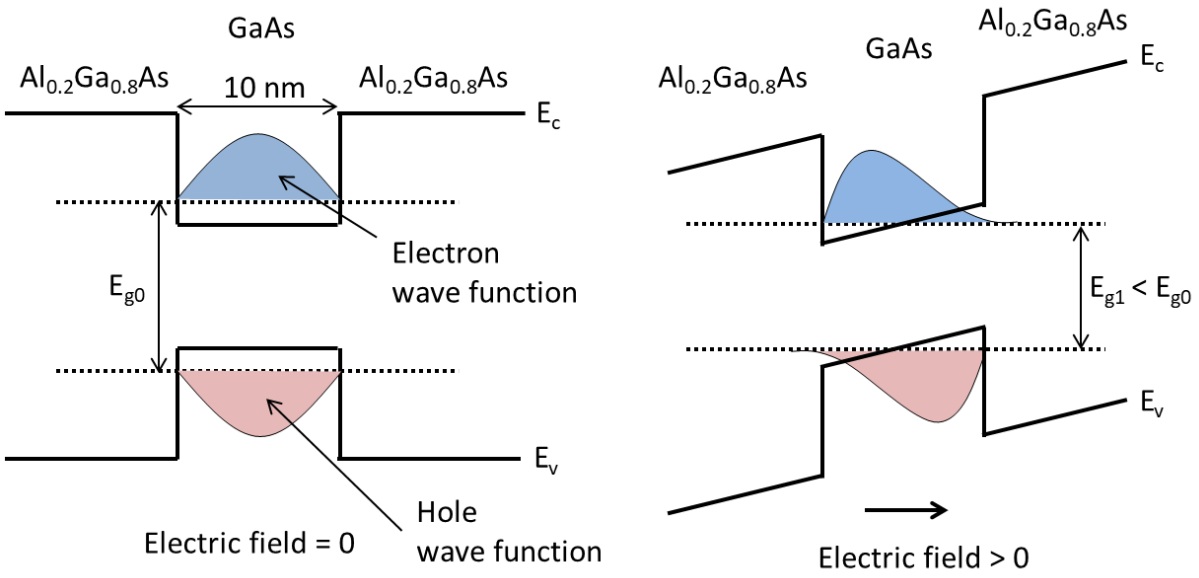

Fig. 5: Schematic band structure of a GaAs–AlGaAs quantum well (left) and tilting of band edges due to an applied electrical field perpendicular to the plane of the quantum well (right). Also indicated are electron and hole wave functions.

also displaces the energies of the bound electron and hole states in such a way that their energy difference becomes smaller, as indicated in the figure. Accordingly the absorption edge shifts towards longer wavelengths, which is known as the QCSE [7]. This effect can be utilized in the design of a low-power, fast absorption modulator. When light whose wavelength corresponds to the absorption peak of the exciton resonance passes through the QW it gets absorbed more when no external field F is applied and is absorbed less when $F > 0$, as the absorption peak shifts towards larger wavelengths. As shown in Sect. 4.2, an optimum operation wavelength has to be found where the absorption change is maximized for a given voltage swing and at the same time the residual transmission loss is small. For a given wavelength, the design of the QW has to be adapted.

3.2 Device structure and fabrication

The fabricated EAM consists of 50 intrinsic 10 nm thick GaAs quantum wells with 10 nm $Al_{0.2}Ga_{0.8}As$ barriers. Since in the first implementation it is to be used as a reflection modulator, an AlAs–$Al_{0.2}Ga_{0.8}As$ Bragg mirror is placed underneath the EAM for reflecting the laser beam. The Bragg reflector is n-doped and has 21 pairs. The two top layers covering the EAM consist of a p-doped 2 µm thick $Al_{0.2}Ga_{0.8}As$ layer and an another p-doped 20 nm thick GaAs layer for protecting the surface. The intrinsic quantum wells are placed between n-doped and p-doped layers in order to get a high field inside the QWs when a reverse bias is applied.

The following fabrication steps are involved for processing the EAM. First a mask is made using photolithography and then reactive ion etching is done on the exposed surface, thereby creating a mesa structure under the mask. Then a p-ring contact consisting of

Ti/Pt/Au (thicknesses of 20 nm / 50 nm / 150 nm) is evaporated. Finally the modulator is cleaved and pasted to the electrical ground of an SMA connector and the top ring contact is wire-bonded to the core of the connector.

4. Device Characterization

4.1 VCSEL

As described in Sect. 3.1, it is necessary to have the right wavelength of operation of the laser that matches with the excitonic absorption peak in order to achieve a high modulation depth of the EAM. In the experiment, a single-mode VCSEL with a peak emission wavelength of around 862 nm is employed which fits well to the EAM, as described in the following section. In a product-type realization of the 3-D sensor, a high-power 2-D VCSEL array should be used.

4.2 EAM

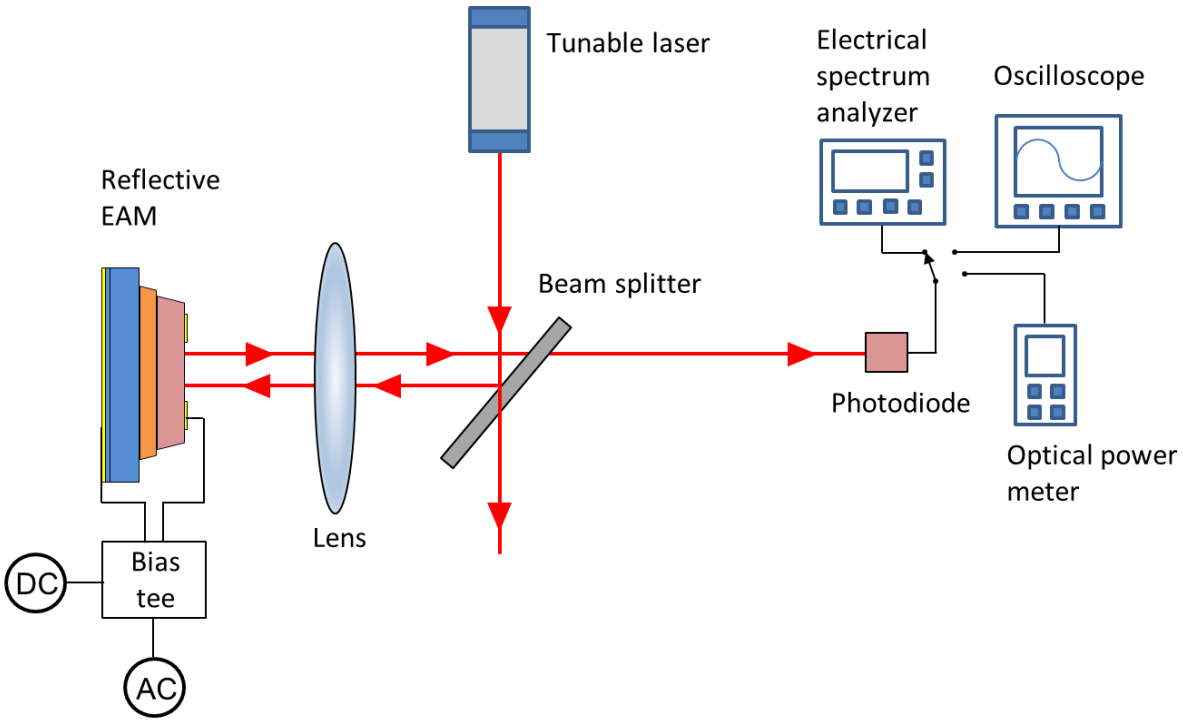

Fig. 6: Setup for EAM characterization.

The setup shown in Fig. 6 is used for characterizing the reflection modulator. A tunable laser with a tuning range from 830 to 880 nm is used as a continuous-wave source. The optical part consists of a lens (5× magnification, NA = 0.1) and a beam splitter. The beam from the tunable laser gets reflected by the beam splitter and is then focused by the lens onto the reflection modulator of dimension 200 µm × 200 µm. The DC bias and

AC signal are added and applied to the modulator through the bias tee. The laser beam is modulated and reflected by the EAM. The light then passes through the beam splitter and is detected by the photodiode. The photodiode can be variably connected to either power meter, oscilloscope, or electrical spectrum analyzer.

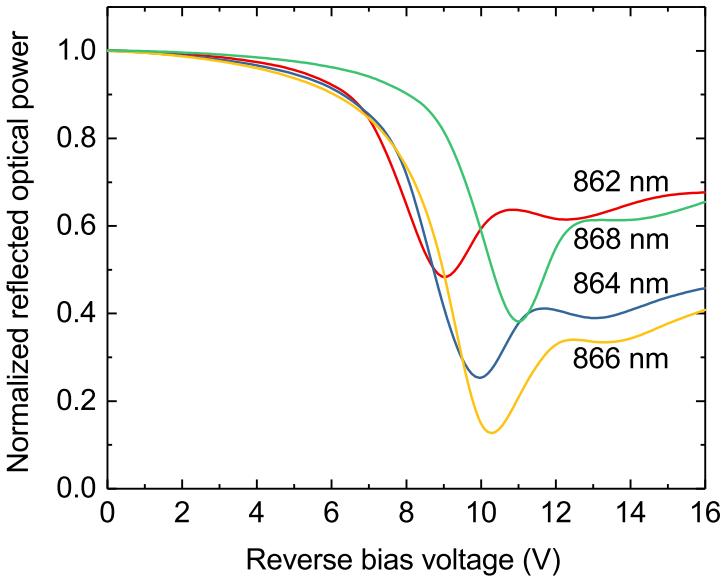

Fig. 7: Normalized reflected light power of a $(200\,\mu\mathrm{m})^2$ size EAM as a function of reverse bias voltage for four different wavelengths of incident tunable laser light.

Figure 7 shows the static characteristics of the modulator which is measured by varying the DC reverse bias without AC signal. The reflected light power is recorded with a power meter. The static characteristics are measured for various wavelengths using the tunable laser. It can be observed that there exists an optimum wavelength for which the modulation depth (difference between highest and the lowest reflectivity) is particularly large. This is due to the fact that maximum absorption occurs when the excitonic peak for an applied voltage coincides with the incident light wavelength. Effects of resonances in the optical cavity formed by the GaAs–air interface and the bottom Bragg mirror also influence the wavelength of maximum modulation depth.

Figure 8 illustrates the dynamic characteristics of the $(200\,\mu\mathrm{m})^2$ size modulator obtained by changing the AC signal frequency for a given DC reverse bias. The measured points are fitted using the first-order low-pass filter function

$$A(f_\mathrm{m}) = -10 \cdot \log_{10}\left[1 + \left(\frac{f_\mathrm{m}}{340.5\,\mathrm{MHz}}\right)^2\right]\,\mathrm{dB}\,. \tag{19}$$

The 3 dB cutoff frequency or corner frequency of the modulator is 340.5 MHz. It is inversely proportional to the RC time constant.The capacitance is directly proportional to the mesa area but inversely proportional to the charge separation distance, i.e., the thickness of the multiple QW region. As discussed in Sect. 2.2, higher frequencies of modulation improve the depth resolution. Smaller area modulators have higher cutoff frequencies but allow less light to pass through and also usually reduce the size of the

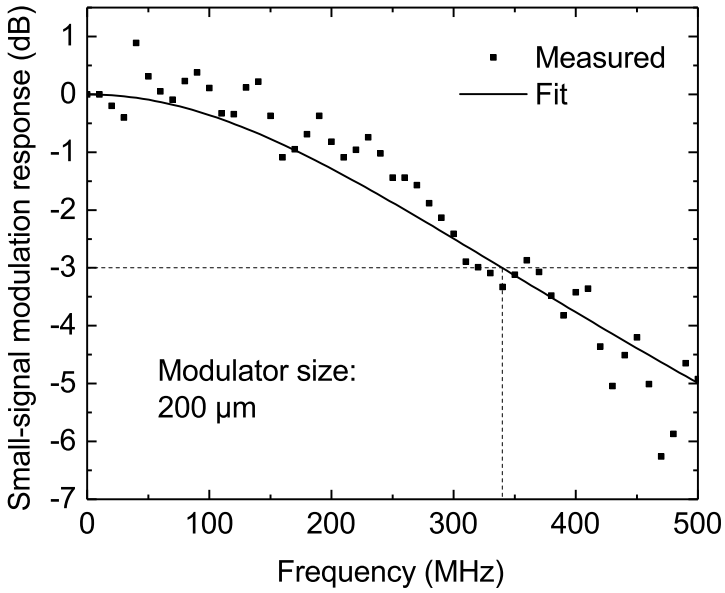

Fig. 8: Small-signal modulation response of a $(200\,\mu\text{m})^2$ size EAM and first-order low-pass fit function according to (19).

image to be captured. On the other hand, larger modulators allow for larger image size but less accurate depth imaging.

5. Conclusion

In summary, various 3-D measurement methods were discussed and a new concept for 3-D imaging was presented. This method uses a sinusoidal modulated VCSEL and a synchronously modulated EAM and works with a regular CMOS camera. Calculations show how distances are determined from measured signals. Static and dynamic characterizations of an EAM were experimentally performed and the optimum operation points of VCSEL and EAM were determined. For high accuracy and precision of the measurements, large modulation amplitude and frequency of both modulated VCSEL and EAM are favorable.

Acknowledgment

The author thanks Philips Photonics GmbH for the MBE growth of the EAM wafer and for providing 860 nm single-mode VCSELs. The author is grateful to Dr. Martin Grabherr for fruitful discussions and valuable suggestions. The technical assistance of Rudolf Rösch, Irene Lamparter, Thomas Zwosta, Susanne Menzel, and Rainer Blood is highly appreciated. Also the author acknowledges Dr. Andreas Trasser and Sven Hettich from the Institute of Electron Devices and Circuits for their help with wire bonding and the signal generators. Last but not least the author expresses his gratitude to Markus Polanik for assisting with reflection spectrum measurements.

References

[1] M. Grzegorzek, C. Theobalt, R. Koch, and A. Kolb (Eds.), *Time-of-Flight and Depth Imaging*, Berlin: Springer-Verlag, 2013.

[2] M. Hansard, S. Lee, O. Choi, and R.P. Horaud, *Time-of-Flight Cameras*, London: Springer, 2013.

[3] J.A. Beraldin, F. Blais, L. Cournoyer, G. Godin, M. Rioux, and J. Taylor, "Active 3D sensing", *IEEE Comput. Graph. Appl.*, vol. 22, pp. 24–35, 2002.

[4] F. Remondino and D. Stoppa (Eds.), *TOF Range-Imaging Cameras*, Berlin: Springer-Verlag, 2016.

[5] R. Michalzik (Ed.), *VCSELs — Fundamentals, Technology and Applications of Vertical-Cavity Surface-Emitting Lasers*, Springer Series in Optical Sciences, vol. 166, Berlin: Springer-Verlag, 2013.

[6] R. Lange and P. Seitz, "Solid-state time-of-flight range camera", *IEEE J. Quantum Electron.*, vol. 37, pp. 390–397, 2001.

[7] D.A.B. Miller, D.S. Chemla, T.C. Damen, A.C. Gossard, W. Wiegmann, T.H. Wood, and C.A. Burrus, "Band-edge electroabsorption in quantum well structures: the quantum-confined Stark effect", *Phys. Rev. Lett.*, vol. 53, pp. 2173–2176, 1984.

[8] C. Kittel, *Introduction to Solid State Physics* (8th ed.), New York: Wiley, 2005.

[9] K.J. Ebeling, *Integrated Optoelectronics*, Berlin: Springer-Verlag, 1993.